HHS Public Access

Author manuscript

Chem Mater. Author manuscript; available in PMC 2020 October 08.

Published in final edited form as:

Chem Mater. 2019 October 8; 31(19): 7845–7854. doi:10.1021/acs.chemmater.9b01750.

Renally Excretable and Size-Tunable Silver Sulfide Nanoparticles for Dual-Energy Mammography or Computed Tomography

Jessica C. Hsu[1,2], **Emma D. Cruz**[1], **Kristen C. Lau**[1,2], **Mathilde Bouché**[1], **Johoon Kim**[1,2], **Andrew D. A. Maidment**[1], **David P. Cormode**[1,2,*]

[1]Department of Radiology, University of Pennsylvania 3400 Spruce St, 1 Silverstein, Philadelphia, PA 19104, USA.

[2]Department of Bioengineering, University of Pennsylvania, Philadelphia, PA, USA.

Abstract

Significant effort has been focused on developing renally-clearable nanoparticle agents since efficient renal clearance is important for eventual clinical translation. Silver sulfide nanoparticles (Ag_2S-NP) have recently been identified as contrast agents for dual energy mammography, computed tomography (CT) and fluorescence imaging and probes for drug delivery and photothermal therapy with good biocompatibility. However, most Ag_2S-NP reported to date are not renally excretable and are observed *in vivo* to accumulate and remain in the reticuloendothelial system (RES) organs, *i.e.* liver and spleen, for a long time, which could negatively impact their likelihood for translation. Herein, we present renally-clearable, 3.1 nm Ag_2S-NP with 85% of the injected dose (ID) being excreted within 24 hours of intravenous injection, which is amongst the best clearance of similarly sized nanoparticles reported thus far (mostly between 20-75% of ID). The urinary excretion and low RES accumulation of these nanoparticles in mice were indicated by in vivo CT imaging and biodistribution analysis. In summary, these ultrasmall Ag_2S-NP can be effectively eliminated via urine and have high translational potential for various biomedical applications.

Graphical Abstract

*Corresponding author david.cormode@uphs.upenn.edu; Tel: 215-615-4656; Fax: 215-662-7868.

Supporting Information

TEM of larger Ag_2S-NP, high-resolution TEM of 3 nm Ag_2S-NP, EDX spectrum, UV-visible absorption spectra, FT-IR spectra, Stability assessment via UV-visible spectroscopy, TEM micrograph of AgNP, CT attenuation (HU) vs. concentration (mg/ml) graphs, CT attenuation rates (HU per mM) graph, *in vivo* CT images of iodine and Ag_2S-NP, TEM micrograph of a urine sample, *in vivo* CT quantification and biodistribution of 90 nm Ag_2S-NP.

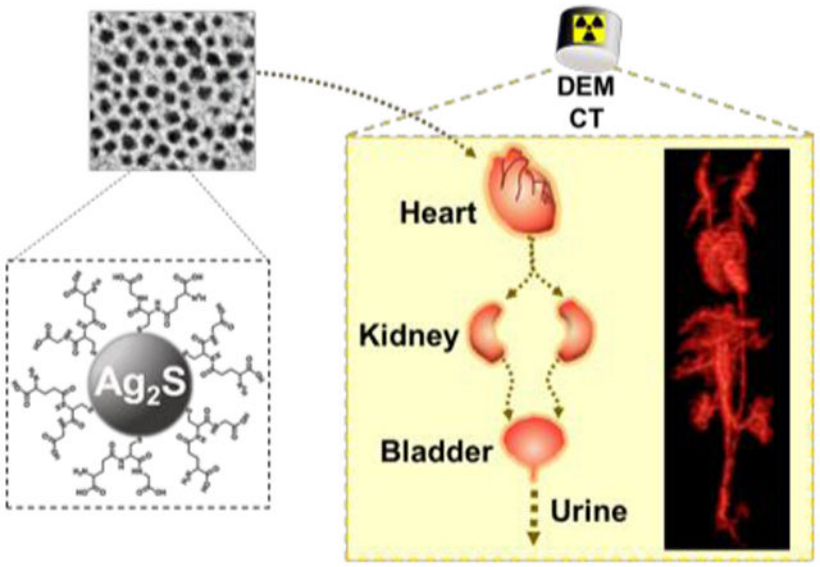

Introduction

The key for potential clinical translation for intravenous contrast agents that include heavy metals is efficient renal clearance.[1] Rapid renal excretion of the agents should avoid safety concerns from long-term retention in the reticuloendothelial system (RES) organs (*i.e.* liver and spleen) and minimize interference with diagnostic results from subsequent screening or monitoring.[2, 3] Efficient clearance is especially important for patients who will receive multiple injections of agent. For example, women with dense breasts, who belong to the very population that is at high risk for breast cancer, are recommended to receive supplemental screening with techniques such as dual energy mammography (DEM), for which iodinated contrast agents are currently used.[4, 5] These women may receive ten or more screenings in their lives, underscoring the importance of the agent being eliminated quickly.

Over the past decade, much effort has been made in developing renally-clearable metal nanoparticles for use in bioimaging applications. Reports have focused on modulating the size, shape, surface charge and composition of quantum dots and gold nanoparticles.[6] Various studies demonstrated that nanoparticles with zwitterionic coating ligands (*i.e.* glutathione and cysteine) and sizes between 1-6 nm have high renal clearance efficiencies.[1, 7, 8] In addition, some studies indicated that renal clearance of nanoparticles is core density-dependent, where greater clearance was observed with lower density particles such as those based on silver.[9, 10]

Recently, silver sulfide nanoparticles (Ag_2S-NP) were reported to be biocompatible, likely due to their very low solubility constant ($K_{sp} = 6.3 \times 10^{-50}$), and have been studied as fluorescence imaging probes and photothermal therapeutic agents as a result of their near-infrared (NIR) optical properties.[11, 12] Furthermore, we have found that silver produces stronger contrast than iodine in DEM and also provides computed tomography (CT) contrast.[13-16] Such nanoparticles would perform well as DEM specific contrast agents when screening for breast cancer. Therefore, the development of renally-clearable Ag_2S-NP would

improve the likelihood of translation and support their use as cancer imaging agents with DEM and CT.

In this study, we report the successful renal clearance of 3.1 nm Ag_2S-NP as evidenced by CT imaging. These nanoparticles were obtained by modulating the reaction time of a viscosity-mediated synthesis that can finely tune the average core sizes between 2 to 10 nm. From biodistribution analysis, we found that 85% of the injected dose (ID) was excreted from the body within 24 hours of intravenous injection, one of the highest clearance efficiencies of similarly sized metal nanoparticles or quantum dots reported to date. A renal clearance efficiency of 20-75% of ID was reported in most previous studies for nanoparticle imaging agents.[6] We also found that these small aqueous Ag_2S-NP have good biocompatibility as observed from *in vitro* cell viability and histopathological assessments. Consequently, these nanoparticles with efficient renal clearance and high translational potential might find applications in imaging with DEM and CT.

Results

Synthesis and characterization of Ag_2S-NP

Hydrophilic, size-tunable Ag_2S-NP were synthesized using a viscosity-mediated, thermal decomposition method, as depicted in Scheme 1.[17] A highly viscous reaction medium was employed to sufficiently reduce the nucleation rate and finely control the growth of the nanoparticles.[18] The reaction was quenched at various time points between 10 and 20 minutes to obtain an array of low dispersity, glutathione-coated silver sulfide nanoparticles with core sizes ranging between 2 to 5 nm, as determined by transmission electron microscopy (TEM) in Fig. 1. TEM of particles with core sizes larger than 5 nm as a result of quenching at later time points are shown in Fig. S1. An electron micrograph of a 3 nm Ag_2S-NP taken by high-resolution TEM is shown in Fig. S2, which indicates lattice fringes (d = 2.60 Å) similar to that with monoclinic Ag_2S phase. Powder X-ray diffraction was used to investigate the crystalline structures of the resultant nanoparticles (Fig. 2). The diffraction peaks become less distinctive and more broad with decreasing nanoparticle size, which is consistent with the results found by others.[19] The characteristic diffraction peaks become apparent with increasing nanoparticle size, and the patterns match well with the monoclinic crystalline structure of Ag_2S and differ from that of pure silver. These nanoparticles have a 2:1 Ag:S stoichiometry as expected (Fig. S3) and possess a broad absorption band (Fig. S4) that is attributed to the electronic properties of Ag_2S-NP. The hydrodynamic diameter (HD) and zeta potential of the differently sized Ag_2S-NP are shown in Table 1. The infrared absorption peak at 2500 cm^{-1} in the Fourier transform infrared spectrum (Fig. S5) which corresponds to free thiol group is absent, suggesting that the glutathione molecules are bound to the nanoparticle surface through the Ag-thiol bond.[20] Notably, no red shift in the absorption spectra, hence no increase in nanoparticle sizes was observed after incubation in PBS or PBS with 10% fetal bovine serum at 37°C for 24 hours as determined by UV/visible spectroscopy (Fig. S6), indicating the stability of these nanoparticles. This can be attributed to the zwitterionic nature of glutathione that provides high stability in biological media and prevents serum protein adsorption, thereby maintaining a small overall size for efficient

renal excretion.[8] For subsequent experiments we used a subset of the synthesized Ag_2S-NP, *i.e.* the 2.3, 3.1 and 5.1 nm nanoparticles.

Silver ion leaching and *in vitro* cytocompatibility

As previously reported, elemental silver nanoparticles are not stable towards oxidation, which can result in the release of silver ions.[21] There is a safety concern over this aspect. We therefore investigated the leaching potential of differently sized Ag_2S-NP when incubated in DI water and citrate buffer at pH 5.[22] Citrate buffer with a low pH was used to mimic the acidic conditions found in lysosomal fluid, the tumor microenvironment and urine.[23] It is particularly important to probe stability at lower pH since silver nanoparticles are often internalized into lysosomes after phagocytosis and are found to release more silver ions under acidic conditions.[24, 25] Of note, chloride-containing media were not used in this study because chloride ions can react with released silver ions to form silver chloride aggregates, preventing the detection of silver ions. A pure silver nanoparticle (AgNP) with the same coating and of comparable size to the Ag_2S-NP (Fig. S7) was used as control.[15] We found that the release of silver ions from AgNP was at least ten-fold higher than Ag_2S-NP of all sizes in both media over 7 days (Fig. 3a-b). The release profiles of the differently sized Ag_2S-NP were not statistically significantly different for either condition. In addition, no significant difference was observed in the release profiles between neutral and acidic pH, demonstrating the stability of these nanoparticles. Overall, our results indicated that Ag_2S-NP (regardless of core size) have minimal silver ion release compared to elemental silver-based nanoparticles due to the ultralow solubility of Ag_2S-NP, which effectively prevents the release of silver ions.

We then assessed the impact of differently sized Ag_2S-NP on the viability of normal kidney (TCMK-1) and liver (AML12) cells (Fig. 3c-d) to probe the effects of silver ion leaching. These cell types were chosen for the study since they should have the greatest exposure to Ag_2S-NP upon injection. Each cell type was incubated with the nanoparticles at the following concentrations for 4 hours: 0.5 and 1.0 mg per ml of Ag. Ag_2S-NP of all sizes were found to be biocompatible with both cell lines at each concentration with no statistically significant differences compared to control. This result is expected since less than 0.1% of the dose was taken up by each cell type at each concentration, and thus, the particles most likely are not significantly endocytosed, which avoids further intracellular interactions and possible cytotoxicity. Furthermore, Ag_2S-NP have minimal silver release and should not have an impact on cell viability regardless of particle size. Nevertheless, since most Ag_2S-NP are expected to be excreted via urine within the first few hours after administration, cellular exposure to these nanoparticles and potential cytotoxicity would be minimized. Overall, our results indicated that Ag_2S-NP have good biocompatibility as a result of minimal silver ion release.

Phantom imaging with CT and DEM

Next, we performed phantom imaging to examine the CT and DEM contrast properties of differently sized Ag_2S-NP. A clinical CT imaging system was used to evaluate the CT attenuation properties of Ag_2S-NP, as silver nanoparticles were previously shown to produce CT contrast.[15, 16] Fig.4a shows the agents produce stronger contrast with increasing

concentrations. Fig. S8 further shows the contrast is linearly correlated with concentration, as is typical in CT.[26] The CT attenuation rates of all agents were calculated and presented in Fig. 4b. CT attenuation rates presented in units of HU per mM are shown in Fig. S9. As expected, the CT attenuation rates of Ag_2S-NP are lower and significantly different than iopamidol at each tube voltage since silver has lower atomic number and hence K-edge energy than iodine. However, no statistical significance was found between the CT attenuation rates of Ag_2S-NP and silver nitrate at each tube voltage. Moreover, the CT attenuation rates among the differently sized Ag_2S-NP were not found to be significantly different, which is consistent with the fact that X-ray absorption is generally related to the material density and atomic number. For all agents, the highest CT attenuation rate occurred at the lowest tube voltage (80 kV) and the rates steadily decreased as the tube voltage increased to 140 kV. The K-edge energies of silver (26 keV) and iodine (33 keV) are at the lower end of each CT energy spectra used, but nearer to the mean photon energy of the low kVp spectrum than high kVp spectrum. This allows for stronger attenuation of lower energy X-rays and results in approximately two-fold higher contrast production when using 80 kVp in comparison with 140 kVp.

A clinical DEM system was used to perform imaging on a gradient ramp phantom. A dual energy (DE) image was created from a logarithmically weighted subtraction of two X-ray images that are acquired at low and high energy.[14] It is evident that the contrast from Ag_2S-NP is greatly enhanced while the variation in background signal is reduced (Fig. 4c). The signal difference-to-noise ratios (SDNR) for PBS, silver salts and three sizes of Ag_2S-NP were calculated from DE images and are presented in Fig. 4d. The results indicate that the signal produced from Ag_2S-NP is significant higher than background breast tissues or PBS, which is consistent with previously published data.[16] Moreover, there is no significant difference in the SDNR produced among all three sizes and silver salts, which is expected since the concentration of silver was held constant in all cases. From these experiments, we conclude that the signal produced in CT and DEM is not affected by the sizes of Ag_2S-NP and these nanoparticles could serve as a CT and DEM contrast agent.

In vivo CT imaging

To non-invasively monitor the distribution profile and clearance potential of Ag_2S-NP, we injected female nude mice with iodine (control) and 3.1 nm Ag_2S-NP at a dose of 250 mg Ag per kg via tail vein and imaged them using a small animal CT scanner at various time points. This core size was chosen for the clearance study since Ag_2S-NP with this size have a HD below 5.5 nm, which is required for renal clearance.[1] The dose used is comparable to that used clinically for iodinated contrast agents.[27, 28] Typically, the minimal dose for CT contrast agents is 100 mg per kg body weight, and the agents are often used at substantially higher doses.[29] In comparison to the Ag_2S-NP treated group, mice injected with iodinated agents had less contrast in the blood (or heart) as more agent was cleared through the kidneys into the bladder immediately after injection (Fig. S10a). On the other hand, vascular contrast and filtration of Ag_2S-NP from the blood via the kidneys were evident in segmented data (Fig. S10b). This indicates that Ag_2S-NP have a much longer blood circulation time than iodine (Fig. S10c). Moreover, the successful renal excretion of these nanoparticles was observed when contrast in the bladder became significantly higher after injection and

remained high throughout the time course (Fig. 5a). The quantification of CT contrast in different organs revealed the contrast in the bladder was highest of all the organs at all time points after injection (Fig. 5b). The contrast in the blood and kidneys gradually decreased over the two-hour period whereas the contrast in the liver and spleen remained at a more constant, higher level than pre-injection. However, the small increase in CT attenuation (< 60 HU) at 2 hours post-injection (p.i.) suggests that a small amount of Ag_2S-NP remained in the RES organs. In addition, a urine sample was collected at 2 hours p.i. and was examined under TEM, which revealed the presence of these nanoparticles (Fig. S11). The nanoparticles found in urine were measured to have an average core diameter of 3.1 ± 0.4 nm, which matched the average core size of injected Ag_2S-NP. Furthermore, we compared the CT attenuation values in the liver and spleen of mice injected with Ag_2S-NP of larger size (90 nm) to confirm the swift excretion of the small Ag_2S-NP.[16] Significantly higher accumulation in the RES organs was evident with 90 nm Ag_2S-NP since their large size prevented kidney filtration and subsequent urinary excretion (Fig. S12a-b). It seems that the uptake in the RES was greatly reduced with the ultrasmall Ag_2S-NP as a result of kidney filtration and urinary excretion.

Pharmacokinetics and biodistribution

To study the pharmacokinetics of Ag_2S-NP, we collected blood samples at various time points after injection and measured the silver concentrations using inductively coupled plasma optical emission spectroscopy (ICP-OES). We determined the circulation half-life to be 86.6 minutes, which is longer than most clinical iodinated agents (they have an average half-life of 13 minutes).[30] In addition, we found that less than 0.2% of ID was detected in the feces collected over 24 hours, indicating that the clearance of Ag_2S-NP through the biliary pathway or GI tract is highly unlikely. This finding suggests that renal excretion is the main elimination route for Ag_2S-NP.

To determine the clearance efficiency of these small Ag_2S-NP, we used ICP-OES to analyze the silver content in the tissues collected at 24 hours after injection. More silver (8-12% of ID per gram of tissue) was found in the RES organs than in other tissues (Fig. 5c), which is consistent with the CT imaging results (although there is a difference in time point). Notably, the level of uptake was significantly lower in comparison with other studies, which an average uptake of more than 30% of ID per gram was observed for non-renally clearable nanoparticles whose sizes are above the kidney filtration threshold (Fig. S12c).[16, 31-34] The remaining carcasses was measured to have less than 0.2% of ID per gram (or 3% of ID) with most retention in the tail (or the site of injection). The tails were analyzed separately from the rest of the carcasses since some agents might remain there for a prolonged period of time due to possible injection errors.[35] From these results, we determined that 85 ± 2% of ID was excreted from the body via urine and feces within 24 hours of intravenous injection. This finding indicates that efficient renal clearance and low body retention can be achieved with these small Ag_2S-NP.

Pathology analysis

The *in vivo* safety of Ag_2S-NP was assessed by histopathological examination of organs (*i.e.* heart, lungs, liver, spleen, kidneys and urinary bladder) that were fixed and stained with

H&E at 24 hours after injection. As shown in Fig. 6, the treated mice did not show any evident histological abnormalities in those organs in comparison with the control population. Interestingly, some nanoparticles are observed in the glomeruli of the kidneys where particles undergo glomerular filtration for elimination via urinary excretion. The *in vivo* safety of ultrasmall, renally-excretable Ag_2S-NP is supported by these preliminary results.

Discussion

Contrast-enhanced DEM has improved sensitivity for women with intermediate and high risk compared with conventional mammography. This technique has recently been approved for clinical use and can be made available with only minor upgrades to existing digital mammography imaging equipment.[4] Currently, X-ray breast imaging is performed with iodinated small molecules. However, due to their small size, these agents have very short half-lives as they are rapidly cleared from the blood through extravasation and kidney filtration, which can be seen from the CT imaging results in Fig. S10a.[30] The rapid contrast washout requires immediate post-injection imaging and high doses. In addition, these agents are nonspecific which leads to systemic vascular permeation and low tumor accumulation. Furthermore, their swift renal filtration can result in contrast-induced nephropathy in patients with kidney disease.[36, 37] Lastly, the contrast produced by these agents in DEM is non-ideal.[14]

Given these limitations, considerable effort in the past decade has been devoted to developing alternative X-ray imaging agents, most of which are novel nanoparticle-based formulations. Nanoparticle contrast agents are more advantageous for cancer screening as they have prolonged circulation times (Fig. S10c) and are known to generate better target to background ratios.[38, 39] They can be conjugated with targeting ligands to increase the amount of contrast material at diseased sites.[40] In particular, silver nanoparticles are an emerging X-ray contrast agent that produces stronger DEM contrast than iodine and provides CT contrast.[13] Only a few contrast materials developed specifically for DEM have been reported to date.[13, 15, 16] However, most of them are not renally excretable due to large size and are observed *in vivo* to remain in the RES organs for a long time, which can prevent their eventual clinical translation and FDA approval.[3, 41]

In this study, we developed sub-5 nm Ag_2S-NP as a DEM and CT contrast agent that have improved biocompatibility and can be excreted renally. Since pure silver nanoparticles are easily oxidized in biological media, we chose silver sulfide as the material due to their very low solubility constant that effectively prevents the release of silver ions, resulting in high stability and biocompatibility. Renal excretion is preferred because this pathway allows nanoparticle contrast agents to be swiftly eliminated from the body, whereas hepatic excretion is a very inefficient and slow elimination process. Urinary clearance of intravascular agents relies mainly on glomerular filtration in the kidneys, which is highly dependent on particle size. Several studies reported that nanoparticles with a HD of 5.5 nm or less, which is below the filtration-size threshold of 6-8 nm, can be rapidly cleared via the urine, thus effectively minimizing uptake by the RES organs and long-term body retention.[1, 8, 42] From *in vivo* CT imaging, we observed significant CT contrast in the bladder and a small increase in CT attenuation in liver and spleen of mice injected with 3.1 nm Ag_2S-NP.

Biodistribution analysis revealed that 15% ID of 3.1 nm Ag_2S-NP remained in the entire body at 24 hours post-injection, and thus we determined that 85% ID was excreted from the body. Other groups have reported a renal clearance efficiency of 50% ID for 2 nm glutathione coated gold nanoparticles, 70% ID for 3 nm silica nanoparticles and 75% ID for 4 nm cysteine coated quantum dots at 24 hours, 48 hours and 4 hours post-injection, respectively.[1, 8, 43] It should be recognized that these reported values were determined using various quantification methods with different levels of accuracy. Some groups obtained their data using fluorescent or radiolabeled nanoparticles, which is often considered semi-quantitative. Our results were obtained using ICP-OES, which provides the highest level of data accuracy by directly measuring the concentrations of the element of interest. Notably, some of the reported clearance values were determined solely from urine samples collected over a period of time and without the analysis of the remaining carcasses. This approach could result in an underestimation or inaccurate representation of the clearance profile. Therefore, the total retention and excretion values reported from our biodistribution study are reliable and indicate that the ultrasmall Ag_2S-NP are indeed renally clearable with low body retention.

Ag_2S-NP were previously reported for use in several biomedical applications including targeted imaging, biosensing, drug delivery and photothermal therapy. They were mostly used as optical imaging probes for having good stability and biocompatibility and size-tunable NIR fluorescence properties. Many studies utilized their fluorescence emission in the second NIR window (950-1350 nm) for imaging of deep tissues and organs without significant effects from tissue absorption and autofluorescence.[44] In addition, they were found to possess photothermal conversion capabilities, which allowed them to serve as a theranostic agent.[45] Moreover, they could be conjugated with targeting peptides or drugs for *in vivo* targeted tumor imaging or disease treatment.[18] Most importantly, most studies found them to be biocompatible as a result of their low solubility product constant. Our study, where we have reported a Ag_2S-NP formulation with high renal clearance efficiency, may have a broader impact due to the above-mentioned biomedical applications.

Our study has limitations, for example we performed the *in vivo* experiments using mice as the initial animal model to study toxicity and excretion of the lead candidate nanoparticle formulation. Further toxicity assessments should be performed in larger species such as dogs or swine in order to gather data for submission to the Investigational New Drug program prior to human clinical studies. While our clearance results are positive, longer biodistribution timepoints (*i.e.* 1 week, 1 month and 6 months) should be assessed to probe any further toxicity or excretion. In addition, serum could be collected from the blood samples and subjected to a clinical chemistry panel to determine the serum biochemistry for any potential toxic effects on organ functions. Lastly, it is important to note that certain degree of polydispersity is always present in the nanoparticle size, which is contrary to small molecule probes that usually have well-defined size or molecular weight. Therefore, any observed renal clearance should be considered as a combined effect that is integrated from a population of slightly differently sized nanoparticles.

In the future, we could study the excretion characteristics of these nanoparticles in a mouse model of chronic kidney dysfunction to confirm their safety and excretion in the presence of

a renal disease. Moreover, we could evaluate the excretion and DEM contrast of these nanoparticles in a murine model of dense mammary tissues as reported by others.[46] We could also synthesize Ag_2S-NP with lower molecular weight zwitterionic ligands to ensure the smallest possible HD for more efficient renal clearance and lower retention. Furthermore, longer circulation times and enhanced tumor accumulation could be achieved by encapsulating these nanoparticles in larger biodegradable polymeric particles.[47] Lastly, Ag_2S-NP may be an ideal contrast agent for the emerging technique of photon-counting digital mammography and future clinical breast CT scanners.[48-50]

Conclusion

In this study, we developed an array of biocompatible, sub-5 nm Ag_2S-NP. *In vivo* CT imaging indicated the successful excretion of 3.1 nm Ag_2S-NP via urine with low accumulation in the RES organs. We found that 85% of the injected dose was excreted within 24 hours of intravenous injection, which is one of the highest clearance values of similarly sized nanoparticle imaging agents reported to date. Therefore, these ultrasmall silver sulfide nanoparticles with efficient renal excretion have potential as safe DEM and CT contrast agents and are highly promising for future clinical translation.

Materials and methods

Materials.

Silver nitrate ($AgNO_3$, 99%), sodium citrate dihydrate, sodium borohydride and L-glutathione (GSH, 98%) were purchased from Sigma-Aldrich (St Louis, MO). Ethylene glycol was purchased from Fisher Scientific (Fair Lawn, NJ). All chemicals were used as received.

Synthesis of aqueous Ag_2S-NP and AgNP.

The method to synthesize water-soluble Ag_2S-NP with tunable core sizes was adapted from previous reports.[17, 18] In brief, a flask containing 40 ml of ethylene glycol was heated to 120 °C. Then, 100 mg $AgNO_3$ and 140 mg GSH (a molar ratio of 4:3) were added to the flask under nitrogen flow. The reaction mixture was kept at this temperature for one minute to form a colorless transparent mixture. A heating mantle coupled with a temperature controller was used to heat the mixture to 165 °C at a heating rate of 20 °C per minute. The mixture gradually turned from colorless to dark brown after 10 minutes of heating. The mixture was quenched by cooling in an ice water bath at different time points (11, 13, 15, 16, 22 and 28 minutes) to obtain Ag_2S-NP with core sizes between 2 and 10 nm. The products were isolated by adding absolute ethanol and centrifuging at 7000 rcf for 10 minutes. Then, the pellet was collected and redispersed in 20 ml of DI water. The nanoparticles were washed three times in DI water using 3 kDa MWCO filtration tubes (Sartorius Stedim Biotech, Germany). The tubes were spun at 4000 rpm for 30 minutes. After the last wash, the buffer was changed to DPBS and the nanoparticles suspension was concentrated to a final volume of 1 ml. Finally, the nanoparticles suspended in DPBS were filtered through a 20 nm membrane to remove any aggregates and stored at 4 °C for use in subsequent experiments.

The method to synthesize water-soluble AgNP was adapted from a previous study.[15] Briefly, 1.25 ml of 0.1 M sodium citrate dihydrate solution and 1.25 ml of 0.1 M silver nitrate were added to 500 ml DI water while stirring. Then, 5 ml of 0.1 M sodium borohydride in DI water was added to the reaction mixture under vigorous stirring for 1 minute. Subsequently, 30 mg GSH dissolved in 5 ml of DI water was added to the mixture, which was gently stirred overnight. The product was washed thrice with DI water and concentrated using 10 kDa MWCO filtration tubes, which were spun at 4000 rpm for 20 minutes. The nanoparticles were suspended in DI water and filtered through a 20 nm membrane to remove aggregates prior to storing at 4 °C for use in subsequent experiments.

Nanoparticle characterization

Transmission electron microscopy.—TEM samples were prepared by dropping 10 μl of diluted Ag_2S-NP samples (2 μl from concentrated stock added to 498 μl DI water) onto Formvar-coated, carbon film-stabilized copper grids (Electron Microscopy Sciences, Hatfield, PA). The grids were dried in air before imaging. All Ag_2S-NP samples were examined using the T12 cryo-electron microscope (FEI Technai) operated at 120 kV. High-resolution TEM imaging was performed using JEM-F200 (JEOL USA, Inc.) operated at 200 kV. ImageJ (National Institutes of Health, Bethesda, MD) was used to measure the core diameter of Ag_2S-NP (from 1000 nanoparticles per sample).

Powder X-ray diffraction.—A Rigaku GiegerFlex D/Max-B X-ray diffractometer operated at 45 kV and 30 mA with a monochromatized Cu Kα radiation wavelength of 1.5406 Å and a scan rate of 2° per minute was used to record the XRD patterns of dried Ag_2S-NP in the range of 20° to 60°.

Energy dispersive X-ray spectroscopy.—Ag_2S-NP samples were completely dried onto an aluminum substrate under vacuum. Their EDX spectra were recorded using a Quanta 600 field emission gun scanning electron microscope (FEI, USA) operated at 15 kV and equipped with EDX detectors (EDAX, Inc.).

Dynamic light scattering and zeta potential.—A Malvern Nano ZS-90 Zetasizer was used to measure the hydrodynamic diameter (HD) and surface charge of Ag_2S-NP samples containing 1 ml of diluted nanoparticle suspension. HD was reported from the number mean. HD and zeta potential measurements were performed at 25 °C.

UV/visible absorption.—A Thermo Scientific Genesys UV/visible spectrophotometer was used to record the UV-visible absorption spectrum of diluted Ag_2S-NP samples. The absorption intensity was normalized to a maximum of 1 across all samples.

Inductively coupled plasma optical emission spectroscopy.—A Spectro Genesis ICP-OES was used to determine the concentrations of silver presented in Ag_2S-NP samples. The samples were prepared as follows: 10 μl of Ag_2S-NP stock solution was first dissolved in 1 ml of nitric acid and then DI water was added to make the final volume to 10 ml. Three replicates per sample were used.

Fourier transform infrared spectroscopy.—A JASCO FT/IR-480 Plus spectrophotometer was used to collect the infrared spectra of Ag_2S-NP and glutathione. The samples were prepared by grinding 2 μL from concentrated Ag_2S-NP stock (40 mg Ag per ml) or glutathione (15 mg) with 100 mg of dried potassium bromide powder and pressing them into compact pellets.

Silver ion leaching assessment.

The silver ion release profiles of different sized Ag_2S-NP were determined according to a previously published procedure.[15, 16] Briefly, Ag_2S-NP or AgNP suspended in DI water (50 μl from a 100 mg Ag per ml stock) were added to a glass vial and the final volume was made to 5 ml with DI water or citrate buffer at pH 5. The vials were incubated at 37 °C. Then, silver ions released from the larger volume were collected using 3 kDa MWCO ultrafiltration tubes over a 7 day period. The silver content was measured using ICP-OES and cumulative release of silver ions (%) for each time point was presented (mean ± SD).

In vitro cell viability assay.

TCMK-1 and AML12 cell lines were used to evaluate the *in vitro* cytotoxicity of Ag_2S-NP. They were cultured according to the instructions from ATCC. The viability was assessed according to a previously published method.[15] In brief, 20000 cells from each cell line were seeded in each well of a 96 well plate. The seeded cells were allowed to stabilize for 24 hours. The cells were then treated with Ag_2S-NP at concentrations of 0 (control), 0.5 and 1 mg Ag per ml for 4 hours. Once the treatment was done, the cells were washed with PBS to remove the nanoparticles and incubated with the MTS assay (Promega, Madison, WI, USA). Then, the absorbance at 490 nm was recorded using a microplate reader. The cell viability relative to control (%) for each concentration and cell line was determined and presented as mean ± SD.

Phantom imaging

Computed tomography.—The method for constructing a CT phantom was reported in a previous study.[26] Iopamidol, $AgNO_3$, and Ag_2S-NP of varying concentrations (0.5 to 10 mg per ml) were loaded into small tubes (0.2 ml volume) and secured in a plastic rack with parafilm. Three replicates were included for each concentration and each agent. The phantom was placed into a plastic bucket that contained water of 21 cm in height. Then, a clinical CT scanner (Siemens SOMATOM Force) was used to scan the phantom and images were acquired with the following settings: field of view (FOV) = 37 × 37 cm, tube current = 360 mA, tube voltage = 80 to 140 kV, slice thickness = 0.5 mm and matrix size = 512 × 512. Image analysis was done using Osirix 64-bit. CT attenuation for each sample tube at each concentration was determined from three different slices and the attenuation rates (HU·ml/mg) were calculated based on this result. The attenuation rates (mean ± SD) of all agents at each voltage are presented.

Dual energy mammography.—Ag_2S-NP were evaluated for their DEM contrast properties using a contrast-embedded gradient ramp phantom that varies continuously from 100% glandular to 100% adipose tissue. In addition, adipose layers were added to the top and bottom of the ramp section to simulate the skin layer of the breast. In brief, samples

prepared at a concentration of 15 mg per ml of silver or iodine were loaded into polyethylene tubes and inserted into the holes of the phantom in the direction of varying glandularity. Three tubes were prepared for each sample (Ag_2S-NP of 2.3 nm, Ag_2S-NP of 3.1 nm, Ag_2S-NP of 5.1 nm, $AgNO_3$, iopamidol, and PBS). Then, images of the phantom were acquired using a Hologic 3Dimensions mammography system, which has a tungsten anode and 70 μm detector. The system is capable of dual-energy (DE) imaging, in which a high-energy (HE) and a low-energy (LE) image are acquired in a single study. DE images of the phantoms were obtained by a weighted logarithmic subtraction of the HE and LE image pairs.[15, 16] The HE images in our study were acquired at 45 kV using a copper filter and 90 mAs. The LE images were acquired at 26 kV using a silver filter and 100 mAs. The technique parameters were chosen based on our previous work imaging silver nanoparticles.[13, 14] Each tube was scanned a total of three times. Analysis of the phantom images was performed using MATLAB. The signal intensity and noise values were measured by selecting rectangular regions of interest for each tube and signal difference-to-noise ratios were calculated according to a previous study.[14] Data are presented as mean ± SD.

In vivo mouse imaging

Animal experiments.—*In vivo* imaging experiments were conducted using 8 weeks old female nude mice (n=4 per group) purchased from Taconic Biosciences (Hudson, NY). After pre-contrast imaging was done, a dose of 250 mg Ag per kg of body weight was administered through the tail vein. As control, iopamidol was injected at the same dose. Isoflurane was used to anesthetize the mice during the imaging experiments.

Computed tomography.—A MicroCAT II small animal CT scanner (Imtek, Inc., Knoxville, TN) was used to image the mice. The mice were scanned at the following time points: 0 (pre-injection), 5, 30, 60 and 120 minutes post injection. The following parameters were used to acquire the images: tube current = 500 μA, tube voltage = 80 kV, voxel size = 100 μm^3, FOV = 51.2 × 76.8 mm and slice thickness = 100 μm. Image reconstruction was done by applying a Shepp-Logan filter and a Feldkamp cone beam correction. Image analysis was done using Osirix 64-bit. CT attenuations for the various organs were measured and averaged from three slices. The change in attenuation from pre-injection scan is presented as mean ± SEM in Hounsfield units.

Pharmacokinetics.

Blood samples were collected *via* retro-orbital bleeding with heparinized capillary tubes at the following time points after injection: 5, 10, 20, 30, 60, 90, 120 and 240 minutes. Each sample was weighed prior to overnight digestion in nitric acid at 75 °C. DI water was then added to the digested samples before measuring the silver content with ICP-OES. Data are presented as mean ± SD. A first-order exponential decay model was used to fit the data and determine the circulation half-life.

Biodistribution.

At 24 hours p.i., mice were sacrificed and blood samples were collected from them. 20 ml of PBS was perfused via the left ventricle and major organs including the heart, lungs, liver, kidneys, spleen and fecal matter were collected. The weights of the organs and remaining

carcasses were recorded. Next, the organs and carcasses were cut into small pieces and immersed in 3 ml of nitric acid for overnight digestion at 75 °C. Then, 7 ml of DI water was added to the digested samples. The samples were filtered before measuring the concentration of silver with ICP-OES. Data are presented as mean ± SEM.

Pathology analysis.

Mice were injected with PBS solution or Ag_2S-NP at a dose of 250 mg Ag per kg and were sacrificed after 24 hours. Their major organs were collected, rinsed with chilled PBS and were cut into 5 to 6 mm thick pieces. Tissue fixation was done by placing the organ pieces in 10% neutral buffered formalin overnight at 4 °C. The tissues were dehydrated with ethanol prior to embedding in paraffin and staining with hematoxylin and eosin (H&E). A digital microscope (Nikon) was used to examine the stained slices.

Statistical analysis.

At least three replicates or three independent experiments were carried in all studies. GraphPad Prism 6 software was used to perform all statistical analyses. The specific statistical tests that were done are written in the figure caption when applicable.

Supplementary Material

Refer to Web version on PubMed Central for supplementary material.

Acknowledgements

This material is based upon work supported by the National Science Foundation Graduate Research Fellowship under Grant No. DGE-1321851 (JCH). Partial support was provided by the NIH (R01 CA227142) and a grant from the Pennsylvania Breast Cancer Coalition (both DPC). This work was carried out in part at the Singh Center for Nanotechnology, part of the National Nanotechnology Coordinated Infrastructure Program, which is supported by the National Science Foundation grant NNCI-1542153. We thank Dr. Douglas Yates and Yanan Yu for their assistance with high-resolution TEM imaging.

References

1. Choi HS; Liu W; Misra P; Tanaka E; Zimmer JP; Itty Ipe B; Bawendi MG; Frangioni JV, Renal Clearance of Quantum Dots. Nat. Biotechnol 2007, 25, 1165–1170. [PubMed: 17891134]
2. Peer D; Karp JM; Hong S; Farokhzad OC; Margalit R; Langer R, Nanocarriers as an Emerging Platform for Cancer Therapy. Nat. Nanotechnol 2007, 2, 751–760. [PubMed: 18654426]
3. De Jong WH; Hagens WI; Krystek P; Burger MC; Sips AJ; Geertsma RE, Particle Size-Dependent Organ Distribution of Gold Nanoparticles after Intravenous Administration. Biomaterials 2008, 29, 1912–1919. [PubMed: 18242692]
4. Dromain C; Thibault F; Diekmann F; Fallenberg EM; Jong RA; Koomen M; Hendrick RE; Tardivon A; Toledano A, Dual-Energy Contrast-Enhanced Digital Mammography: Initial Clinical Results of a Multireader, Multicase Study. Breast Cancer Res. 2012, 14, R94. [PubMed: 22697607]
5. Yu S-B; Watson AD, Metal-Based X-Ray Contrast Media. Chem. Rev 1999, 99, 2353–2378. [PubMed: 11749484]
6. Du B; Yu M; Zheng J, Transport and Interactions of Nanoparticles in the Kidneys. Nat. Rev. Mater 2018, 3, 358–374.
7. Choi HS; Ipe BI; Misra P; Lee JH; Bawendi MG; Frangioni JV, Tissue- and Organ-Selective Biodistribution of NIR Fluorescent Quantum Dots. Nano Lett 2009, 9, 2354–2359. [PubMed: 19422261]

8. Zhou C; Long M; Qin Y; Sun X; Zheng J, Luminescent Gold Nanoparticles with Efficient Renal Clearance. Angew. Chem., Int. Ed 2011, 50, 3168–3172.
9. Tang S; Peng C; Xu J; Du B; Wang Q; Vinluan RD 3rd; Yu M; Kim MJ; Zheng J, Tailoring Renal Clearance and Tumor Targeting of Ultrasmall Metal Nanoparticles with Particle Density. Angew. Chem. Int. Ed. Engl 2016, 55, 16039–16043. [PubMed: 27882633]
10. Zhou M; Li J; Liang S; Sood AK; Liang D; Li C, CuS Nanodots with Ultrahigh Efficient Renal Clearance for Positron Emission Tomography Imaging and Image-Guided Photothermal Therapy. ACS Nano 2015, 9, 7085–7096. [PubMed: 26098195]
11. Levard C; Hotze EM; Colman BP; Dale AL; Truong L; Yang XY; Bone AJ; Brown GE; Tanguay RL; Di Giulio RT; Bernhardt ES; Meyer JN; Wiesner MR; Lowry GV, Sulfidation of Silver Nanoparticles: Natural Antidote to Their Toxicity. Environ. Sci. Technol 2013, 47, 13440–13448. [PubMed: 24180218]
12. Lu C; Chen G; Yu B; Cong H, Recent Advances of Low Biological Toxicity Ag_2S QDs for Biomedical Application. Adv. Eng. Mater 2018, 20, 1700940.
13. Karunamuni R; Naha PC; Lau KC; Al-Zaki A; Popov AV; Delikatny EJ; Tsourkas A; Cormode DP; Maidment AD, Development of Silica-Encapsulated Silver Nanoparticles as Contrast Agents Intended for Dual-Energy Mammography. Eur. J. Radiol 2016, 26, 3301–3309.
14. Karunamuni R; Tsourkas A; Maidment AD, Exploring Silver as a Contrast Agent for Contrast-Enhanced Dual-Energy X-Ray Breast Imaging. Br. J. Radiol 2014, 87, 20140081. [PubMed: 24998157]
15. Naha PC; Lau KC; Hsu JC; Hajfathalian M; Mian S; Chhour P; Uppuluri L; McDonald ES; Maidment AD; Cormode DP, Gold Silver Alloy Nanoparticles (GSAN): An Imaging Probe for Breast Cancer Screening with Dual-Energy Mammography or Computed Tomography. Nanoscale 2016, 8, 13740–13754. [PubMed: 27412458]
16. Hsu JC; Naha PC; Lau KC; Chhour P; Hastings R; Moon BF; Stein JM; Witschey WRT; McDonald ES; Maidment ADA; Cormode DP, An All-In-One Nanoparticle (AION) Contrast Agent for Breast Cancer Screening with DEM-CT-MRI-NIRF Imaging. Nanoscale 2018, 10, 17236–17248. [PubMed: 30191237]
17. Tan L; Wan A; Li H, Ag_2S Quantum Dots Conjugated Chitosan Nanospheres toward Light-Triggered Nitric Oxide Release and Near-Infrared Fluorescence Imaging. Langmuir 2013, 29, 15032–15042. [PubMed: 24224470]
18. Tang R; Xue J; Xu B; Shen D; Sudlow GP; Achilefu S, Tunable Ultrasmall Visible-to-Extended Near-Infrared Emitting Silver Sulfide Quantum Dots for Integrin-Targeted Cancer Imaging. ACS Nano 2015, 9, 220–230. [PubMed: 25560768]
19. Zhang Y; Liu Y; Li C; Chen X; Wang Q, Controlled Synthesis of Ag_2S Quantum Dots and Experimental Determination of the Exciton Bohr Radius. J. Phys. Chem. C 2014, 118, 4918–4923.
20. Jiang P; Zhu CN; Zhang ZL; Tian ZQ; Pang DW, Water-Soluble Ag_2S Quantum Dots for Near-Infrared Fluorescence Imaging in Vivo. Biomaterials 2012, 33, 5130–5135. [PubMed: 22484042]
21. Levard C; Hotze EM; Lowry GV; Brown GE Jr., Environmental Transformations of Silver Nanoparticles: Impact on Stability and Toxicity. Environ. Sci. Technol 2012, 46, 6900–6914. [PubMed: 22339502]
22. Naha PC; Zaki AA; Hecht E; Chorny M; Chhour P; Blankemeyer E; Yates DM; Witschey WR; Litt HI; Tsourkas A; Cormode DP, Dextran Coated Bismuth-Iron Oxide Nanohybrid Contrast Agents for Computed Tomography and Magnetic Resonance Imaging. J. Mater. Chem. B 2014, 2, 8239–8248. [PubMed: 25485115]
23. Hasegawa R; Cohen SM, The Effect of Different Salts of Saccharin on the Rat Urinary Bladder. Cancer Lett. 1986, 30, 261–268. [PubMed: 3697946]
24. Liu J; Hurt RH, Ion Release Kinetics and Particle Persistence in Aqueous Nano-Silver Colloids. Environ. Sci. Technol 2010, 44, 2169–2175. [PubMed: 20175529]
25. Loza K; Diendorf J; Sengstock C; Ruiz-Gonzalez L; Gonzalez-Calbet JM; Vallet-Regi M; Koller M; Epple M, The Dissolution and Biological Effects of Silver Nanoparticles in Biological Media. J. Mater. Chem. B 2014, 2, 1634–1643. [PubMed: 32261391]

26. Galper MW; Saung MT; Fuster V; Roessl E; Thran A; Proksa R; Fayad ZA; Cormode DP, Effect of Computed Tomography Scanning Parameters on Gold Nanoparticle and Iodine Contrast. Invest. Radiol 2012, 47, 475–481. [PubMed: 22766909]
27. Halpern EJ; Gingold EL; White H; Read K, Evaluation of Coronary Artery Image Quality with Knowledge-Based Iterative Model Reconstruction. Acad. Radiol 2014, 21, 805–811. [PubMed: 24809321]
28. Luczynska E; Heinze-Paluchowska S; Hendrick E; Dyczek S; Rys J; Herman K; Blecharz P; Jakubowicz J, Comparison between Breast MRI and Contrast-Enhanced Spectral Mammography. Med. Sci. Monit 2015, 21, 1358–1367. [PubMed: 25963880]
29. Yeh BM; FitzGerald PF; Edic PM; Lambert JW; Colborn RE; Marino ME; Evans PM; Roberts JC; Wang ZJ; Wong MJ; Bonitatibus PJ Jr., Opportunities for New CT Contrast Agents to Maximize the Diagnostic Potential of Emerging Spectral CT Technologies. Adv. Drug Delivery Rev 2017, 113, 201–222.
30. Dean PB; Kivisaari L; Kormano M, Contrast Enhancement Pharmacokinetics of Six Ionic and Nonionic Contrast Media. Invest. Radiol 1983, 18, 368–374. [PubMed: 6618828]
31. Hajfathalian M; Amirshaghaghi A; Naha PC; Chhour P; Hsu JC; Douglas K; Dong Y; Sehgal CM; Tsourkas A; Neretina S; Cormode DP, Wulff in a Cage Gold Nanoparticles as Contrast Agents for Computed Tomography and Photoacoustic Imaging. Nanoscale 2018, 10, 18749–18757. [PubMed: 30276391]
32. Hong G; Robinson JT; Zhang Y; Diao S; Antaris AL; Wang Q; Dai H, In Vivo Fluorescence Imaging with Ag_2S Quantum Dots in the Second Near-Infrared Region. Angew. Chem., Int. Ed 2012, 51, 9818–9821.
33. Lipka J; Semmler-Behnke M; Sperling RA; Wenk A; Takenaka S; Schleh C; Kissel T; Parak WJ; Kreyling WG, Biodistribution of PEG-Modified Gold Nanoparticles Following Intratracheal Instillation and Intravenous Injection. Biomaterials 2010, 31, 6574–6581. [PubMed: 20542560]
34. Zhang G; Yang Z; Lu W; Zhang R; Huang Q; Tian M; Li L; Liang D; Li C, Influence of Anchoring Ligands and Particle Size on the Colloidal Stability and in Vivo Biodistribution of Polyethylene Glycol-Coated Gold Nanoparticles in Tumor-Xenografted Mice. Biomaterials 2009, 30, 1928–1936. [PubMed: 19131103]
35. Groman EV; Reinhardt CP, Method to Quantify Tail Vein Injection Technique in Small Animals. Contemp. Top. Lab. Anim. Sci 2004, 43, 35–38.
36. Tepel M; Aspelin P; Lameire N, Contrast-Induced Nephropathy: A Clinical and Evidence-Based Approach. Circulation 2006, 113, 1799–1806. [PubMed: 16606801]
37. Weisberg LS; Kurnik PB; Kurnik BR, Risk of Radiocontrast Nephropathy in Patients with and without Diabetes Mellitus. Kidney international 1994, 45, 259–265. [PubMed: 8127017]
38. Al Zaki A; Joh D; Cheng Z; De Barros AL; Kao G; Dorsey J; Tsourkas A, Gold-Loaded Polymeric Micelles for Computed Tomography-Guided Radiation Therapy Treatment and Radiosensitization. ACS Nano 2014, 8, 104–112. [PubMed: 24377302]
39. Cormode DP; Skajaa T; van Schooneveld MM; Koole R; Jarzyna P; Lobatto ME; Calcagno C; Barazza A; Gordon RE; Zanzonico P; Fisher EA; Fayad ZA; Mulder WJ, Nanocrystal Core High-Density Lipoproteins: A Multimodality Contrast Agent Platform. Nano Lett. 2008, 8, 3715–3723. [PubMed: 18939808]
40. Vlashi E; Kelderhouse LE; Sturgis JE; Low PS, Effect of Folate-Targeted Nanoparticle Size on Their Rates of Penetration into Solid Tumors. ACS Nano 2013, 7, 8573–8582. [PubMed: 24020507]
41. Sonavane G; Tomoda K; Makino K, Biodistribution of Colloidal Gold Nanoparticles after Intravenous Administration: Effect of Particle Size. Colloids Surf., B 2008, 66, 274–280.
42. Hainfeld JF; Slatkin DN; Focella TM; Smilowitz HM, Gold Nanoparticles: A New X-Ray Contrast Agent. Br. J. Radiol 2006, 79, 248–253. [PubMed: 16498039]
43. Burns AA; Vider J; Ow H; Herz E; Penate-Medina O; Baumgart M; Larson SM; Wiesner U; Bradbury M, Fluorescent Silica Nanoparticles with Efficient Urinary Excretion for Nanomedicine. Nano Lett. 2009, 9, 442–448. [PubMed: 19099455]

44. Zhang Y; Zhang Y; Hong G; He W; Zhou K; Yang K; Li F; Chen G; Liu Z; Dai H; Wang Q, Biodistribution, Pharmacokinetics and Toxicology of Ag_2S Near-Infrared Quantum Dots in Mice. Biomaterials 2013, 34, 3639–3646. [PubMed: 23415643]
45. Yang T; Tang Y; Liu L; Lv X; Wang Q; Ke H; Deng Y; Yang H; Yang X; Liu G; Zhao Y; Chen H, Size-Dependent Ag_2S Nanodots for Second Near-Infrared Fluorescence/Photoacoustics Imaging and Simultaneous Photothermal Therapy. ACS Nano 2017, 11, 1848–1857. [PubMed: 28117993]
46. Cole LE; Vargo-Gogola T; Roeder RK, Contrast-Enhanced X-Ray Detection of Microcalcifications in Radiographically Dense Mammary Tissue Using Targeted Gold Nanoparticles. ACS Nano 2015, 9, 8923–8932. [PubMed: 26308767]
47. Cheheltani R; Ezzibdeh RM; Chhour P; Pulaparthi K; Kim J; Jurcova M; Hsu JC; Blundell C; Litt HI; Ferrari VA; Allcock HR; Sehgal CM; Cormode DP, Tunable, Biodegradable Gold Nanoparticles as Contrast Agents for Computed Tomography and Photoacoustic Imaging. Biomaterials 2016, 102, 87–97. [PubMed: 27322961]
48. Lindfors KK; Boone JM; Nelson TR; Yang K; Kwan AL; Miller DF, Dedicated Breast CT: Initial Clinical Experience. Radiology 2008, 246, 725–733. [PubMed: 18195383]
49. Erhard K; Kilburn-Toppin F; Willsher P; Moa E; Fredenberg E; Wieberneit N; Buelow T; Wallis MG, Characterization of Cystic Lesions by Spectral Mammography: Results of a Clinical Pilot Study. Invest. Radiol 2016, 51, 340–347. [PubMed: 26741891]
50. Fredenberg E; Kilburn-Toppin F; Willsher P; Moa E; Danielsson M; Dance DR; Young KC; Wallis MG, Measurement of Breast-Tissue X-Ray Attenuation by Spectral Mammography: Solid Lesions. Phys. Med. Biol 2016, 61, 2595–2612. [PubMed: 26961507]

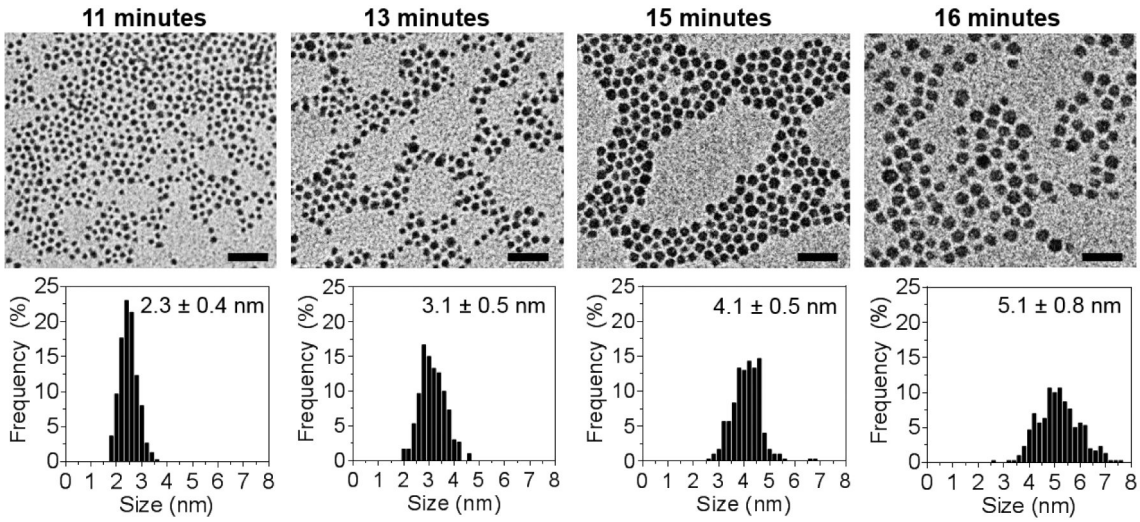

Figure 1.

Representative TEM images and core size distributions showing size tunability of Ag_2S-NP based on reaction time. All scale bars are 20 nm.

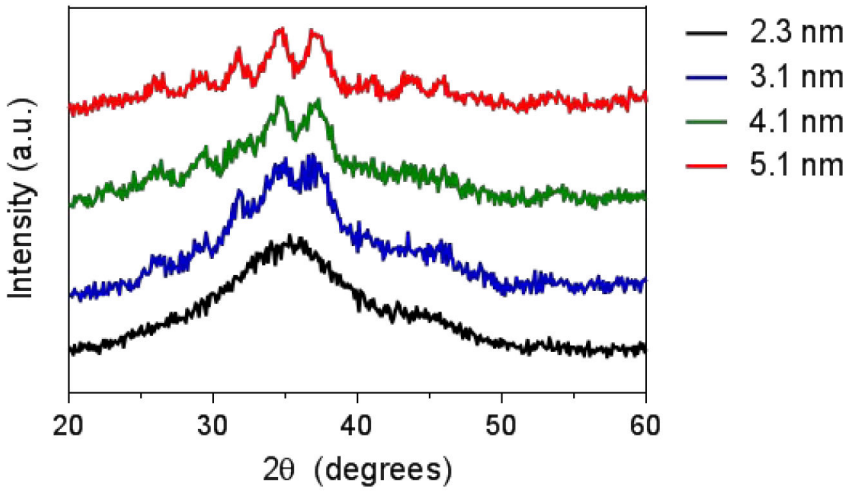

Figure 2.
X-ray diffraction patterns of Ag_2S-NP of different sizes.

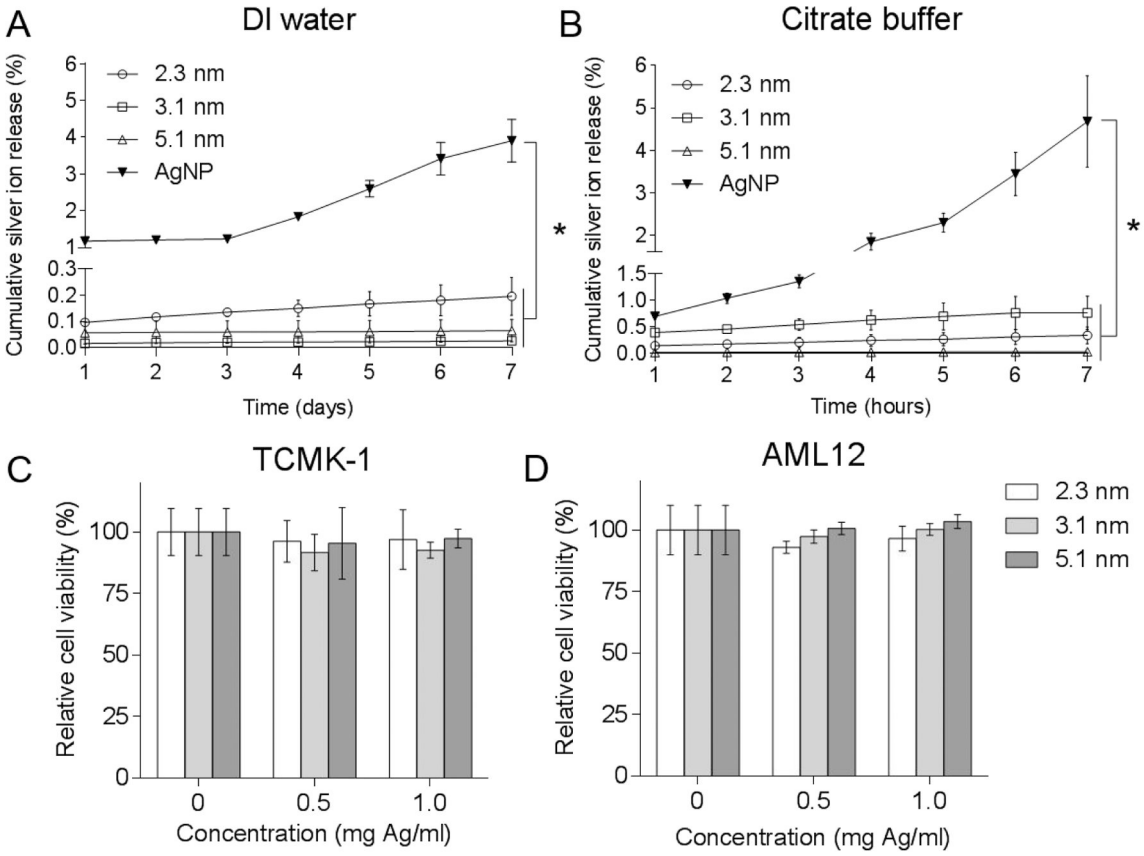

Figure 3.

Silver ion release from Ag_2S-NP of different core diameters and AgNP when incubated in (A) DI water and (B) citrate buffer of pH 5 at 37 °C over a 7-day period. Viability of (C) TCMK-1 and (D) AML12 cells when incubated with Ag_2S-NP for 4 hours. * indicates $P < 0.05$ compared to control (two way ANOVA with Bonferroni's multiple comparisons test). Error bars are one standard deviation. Some error bars are smaller than the data point marker and are thus not visible.

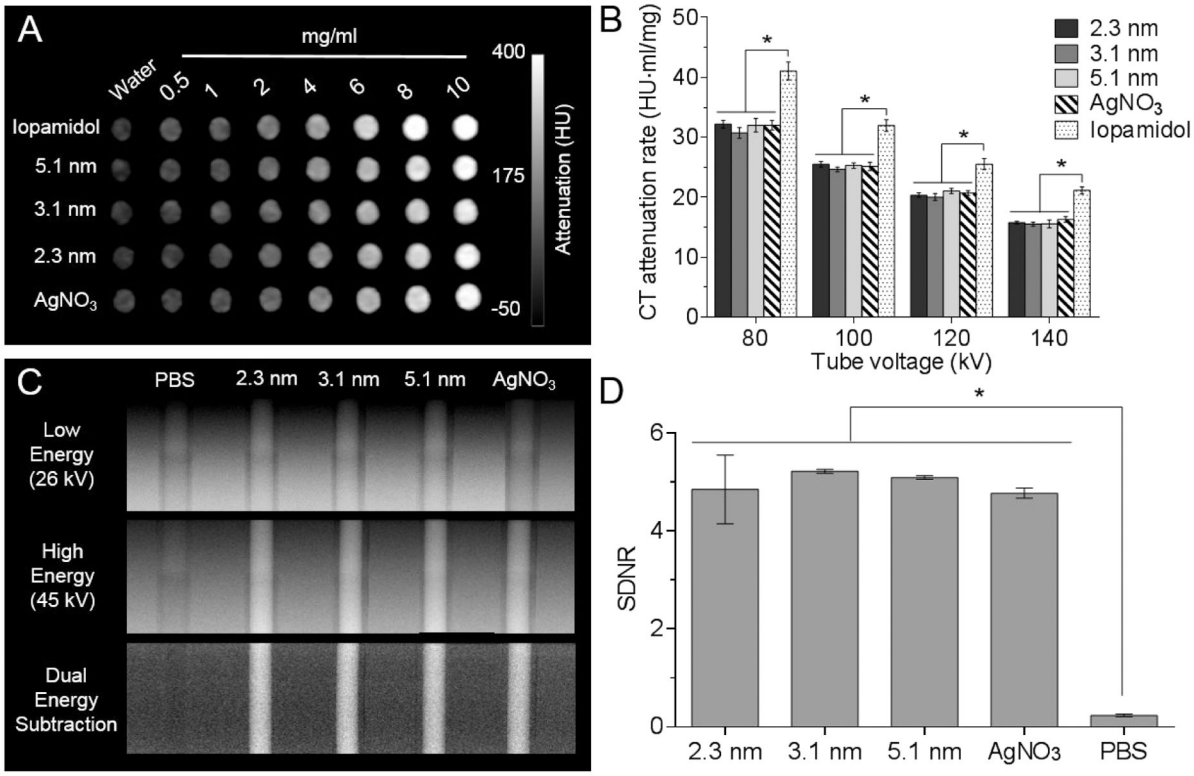

Figure 4.

Phantom imaging of different agents with DEM and CT. (A) CT phantom image at 80 kV and (B) CT attenuation rates for each tube voltage. (C) DEM phantom images and (D) signal difference-to-noise ratios calculated from DE subtraction images in (C). Error bars are one standard deviation in all cases. * indicates $P < 0.05$ (two-way ANOVA and one-way ANOVA for panels B and D, respectively, with Tukey's multiple comparisons tests).

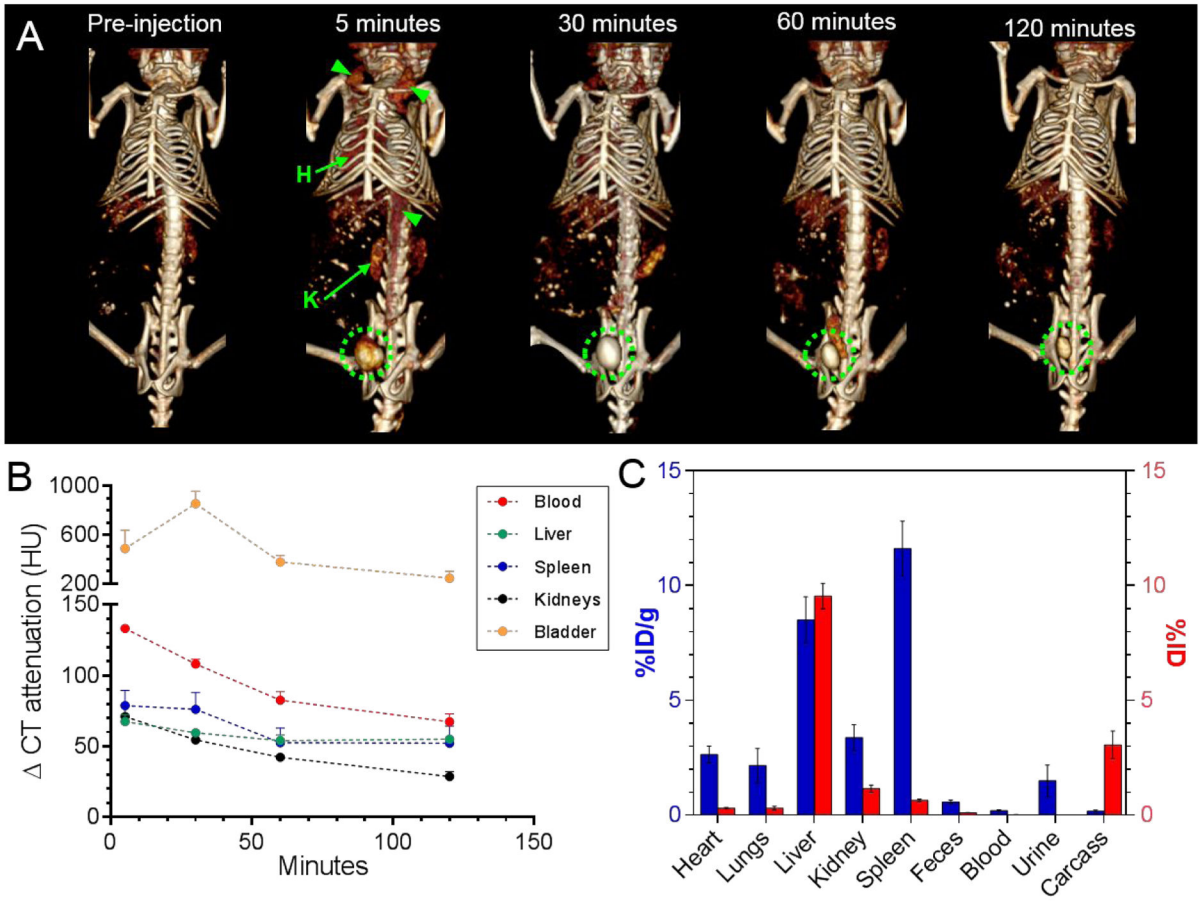

Figure 5.

(A) Representative 3D volume rendered CT images of a mouse injected with Ag_2S-NP that have an average core diameter of 3.1 nm. The images are shown with a window level of 500 HU and window width of 200 HU. Green arrowheads mark the blood vessels and green circles indicate the bladder. Hearts and kidneys are labeled H and K, respectively. Some attenuation from food minerals were observed in the abdomen before injection. (B) The change in CT attenuation in different organs of mice at different time points compared to pre-injection. (C) Biodistribution of Ag_2S-NP with an average core size of 3.1 nm in major organs and remaining carcasses at 24 hours p.i. as determined by ICP-OES. The values are given in units of %ID per gram and %ID as indicated by the blue (left y-axis) and red (right y-axis) bars, respectively. Error bars are standard error of mean. Some error bars are smaller than the data point marker and are thus not visible.

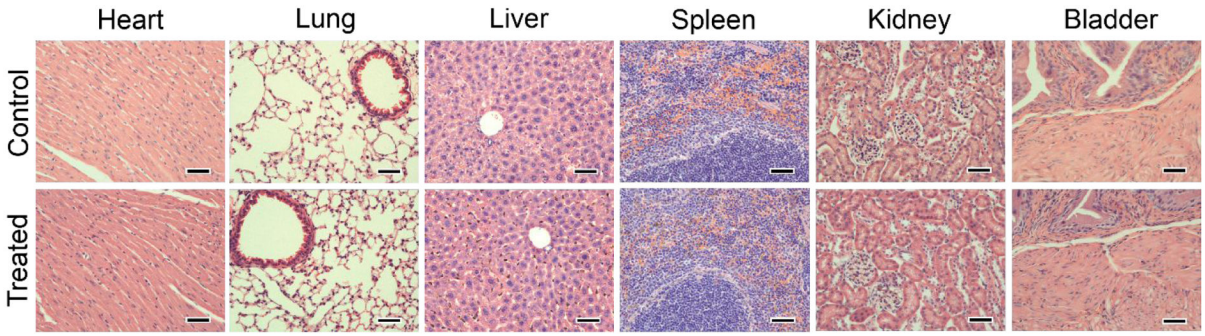

Figure 6.

Representative H&E stained micrographs of organs including heart, lung, liver, spleen, kidney and bladder from mice injected with PBS (control) or Ag_2S-NP (treated). The dose of Ag_2S-NP was 250 mg Ag per kg. The treated mice did not show any apparent organ damages or lesions as compared to the control. Scale bar = 50 μm.

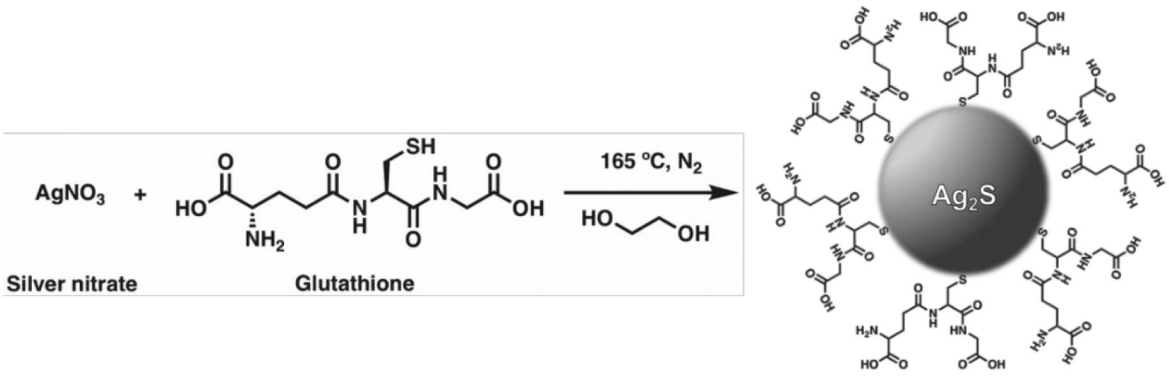

Scheme 1.

Synthesis of water-soluble glutathione-coated Ag_2S-NP with tunable sizes.

Table 1.

Characterization data for Ag_2S-NP synthesized using differing reaction times.

Reaction Time (minutes)	TEM Diameter (nm)	DLS		Surface charge (mV)
		HD (nm)	PDI	
16	5.1 ± 0.8	7.4 ± 1.0	0.20	−18 ± 3
15	4.1 ± 0.5	6.8 ± 2.2	0.37	−15 ± 3
13	3.1 ± 0.5	4.9 ± 1.0	0.46	−11 ± 2
11	2.3 ± 0.4	3.9 ± 1.0	0.60	−7 ± 1